Crystals 2022

MDPI

Proceedings

Fabrication and characterization of ethylammonium- and rubidium-added perovskite solar cells †

Keinoshin Takada [1], Takeo Oku [1,*], Atsushi Suzuki [1], Masanobu Okita [2], Sakiko Fukunishi [2], Tomoharu Tachikawa [2], Tomoya Hasegawa [2]

[1] Department of Materials Science, The University of Shiga Prefecture, 2500 Hassaka, Hikone, Shiga 522-8533, Japan; oe21ktakada@ec.usp.ac.jp (K.T.); suzuki@mat.usp.ac.jp (A.S.)
[2] Osaka Gas Chemicals Co., Ltd., 5-11-61 Torishima, Konohana-ku, Osaka 554-0051, Japan; okita@ogc.co.jp (M.O.); fukunishi@ogc.co.jp (S.F.); t-tachikawa@ogc.co.jp (T.T.); hasegawa_tomoya@ogc.co.jp (T.H.)
* Correspondence: oku@mat.usp.ac.jp; Tel.: +81-749-28-8368

Abstract: Conversion efficiencies and stability of the perovskite solar cells were improved by adding a small amount of ethylammonium (EA) and rubidium (Rb) to the $CH_3NH_3PbI_3$ compounds. Addition of ethylamine hydrobromide and rubidium iodide provided an increase in carrier concentration and promotion of crystal growth, resulting in an improvement in conversion efficiencies and stability. First-principles calculations showed that the addition of Rb lowered the total energy and made the crystal stable. The band calculation also shows that the EA addition reduce the effective mass and improves the carrier mobility.

Keywords: perovskite; solar cell; photovoltaic device; rubidium; ethylammonium; first-principles calculation; band calculation

1. Introduction

In order to solve the problems of global warming and energy resources, the use of renewable energy sources is being promoted. One of them is a solar cell that uses light energy from the sun. One of the solar cells is called perovskite solar cells [1,2], which use materials with a crystalline structure called perovskite for the photoactive layer and have high conversion efficiencies comparable to silicon solar cells currently in circulation [3]. The perovskite solar cells have the advantage of lower cost than silicon solar cells because they can be produced using coating technology [4,5]. In addition, flexible and light-weight solar cells can be realized, making it possible to install them in places where silicon solar cells are difficult to install [6-9].

Perovskite solar cells are widely studied, and the partial substitution method with different elements and molecules is often used to improve the properties of perovskite solar cells [10-12].Organic–inorganic metal halide perovskites have a cubic structure with a general formula ABX_3, where A is an organic cation, B is a divalent metal ion, and X is a halide ion [13-17]. Doping with elements such as cesium, rubidium (Rb) [15,18,19], potassium [20,21], sodium [22], formamidinium ($CH(NH_2)_2$, FA) [23], ethylammonium ($CH_3CH_2NH_3$, EA) [24-26], or guanidinium ($C(NH_2)_3$, GA) [27-29] at the methylammonium (CH_3NH_3, MA) sites improved the conversion efficiencies. Studies on doping with halogen atoms, such as chlorine (Cl) or bromine (Br), at the iodine (I) sites of the perovskite crystals have also been reported [17,30]. Pb-free and large grain perovskite solar cells have also been investigated [31-35].

The purpose of this study is to investigate the photovoltaic properties of perovskite layers by adding EA and Rb. It is reported that the addition of EA improves the surface morphology of the perovskite layer, and the addition of Rb generates more carriers but

Citation: Lastname, F.; Lastname, F.; Lastname, F. Title. *Chem. Proc.* **2021**, *3*, x. https://doi.org/10.3390/xxxxx

Published: date

also causes defects in the perovskite layer [2,3]. The effect of these additives on the formation of perovskite compounds in solar cells was investigated using current density - voltage curves, external quantum efficiencies (EQE), X-ray diffraction (XRD) patterns, and scanning electron microscope **(**SEM) images and elemental mapping images. First-principles calculations were also used for band calculations and comparison according to the density of states.

2. Experimental

A schematic illustration of the present perovskite photovoltaic cells is shown in Figure 1. F-doped tin oxide (FTO) substrates were cleaned in an ultrasonic bath with acetone and methanol and dried under nitrogen gas. The 0.15 and 0.30 M TiO_2 precursor soltions were prepared from titanium diisopropoxide bis (acetylacetonate) (0.055 and 0.11 mL) with 1-butanol (1 mL), and the 0.15 M TiO_2 precursor solution was spin-coated on the FTO substrate at 3000 rpm for 30 s and heated at 125 °C for 5 min in air to form a TiO_x layer [36]. The 0.30 M TiO_2 precursor solution was spin-coated onto the TiO_x layer at 3000 rpm for 30 s, and heated at 125 °C for 5 min. This process of coating with a 0.30 M solution was then performed two times, and the FTO substrate was annealed at 550 °C for 30 min to form a compact TiO_2 layer. For the mesoporous TiO_2 layer, TiO_2 paste was prepared with TiO_2 powder with poly in ultrapure water. The solution was mixed with acetylacetone (10 μL) and triton X-100 (5 μL) for 30 min, and then left for 12 h to suppress the bubbles in the solution. After that, the TiO_2 paste was coated onto the substrate by spin-coating at 5000 rpm for 30 s. The cells were then annealed at 120 °C for 5 min and at 550 °C for 30 min to form a mesoporous TiO_2 layer.

For the preparation of perovskite compounds, a solution of CH_3NH_3I (190.7 mg) and $PbCl_2$ (111.2 mg) was prepared with a mole ratio of 3:1 and in N,N-dimethylformamide (500 μL) with additives of EABr and RbI . These perovskite solutions were spin-coated three times at 2000 rpm for 60 s [37]. During the third spin-coating, several drops of DPPS were added [38-41], which is effective for the formation of stable devices [42].

A hole-transport layer was prepared by spin-coating. A solution of spiro-OMeTAD (50 mg) in chlorobenzene (0.5 mL) was mixed with a solution of lithium bis (tri-fluoromethylsulfonyl) imide (260 mg) in acetonitrile (0.5 mL) for 24 h. The former solution with 4-tertbutylpyridine (14.4 mL) was mixed with the Li-TFSI solution (8.8 mL) for 30 min at 70 °C. Then, the spiro-OMeTAD solution was spin-coated on the perovskite layer at 4000 rpm for 30 s. All procedures were performed in ambient air. Finally, gold (Au) electrodes were evaporated as top electrodes using a metal mask for the patterning.

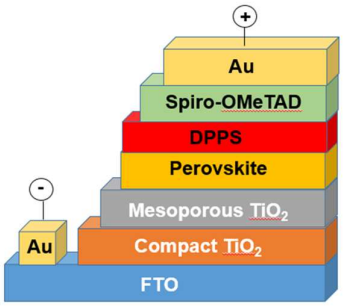

Figure 1. Layered structure of the present solar cells.

3. Results and Discussion

Figure 2 shows the electron density distribution of $MA_{0.625}EA_{0.25}Rb_{0.125}PbI_{2.25}Br_{0.75}$, showing that the electron density is higher around Br compared with I. It can also be seen that the electrons are delocalized in MA and EA, and there are almost no electrons around Rb.

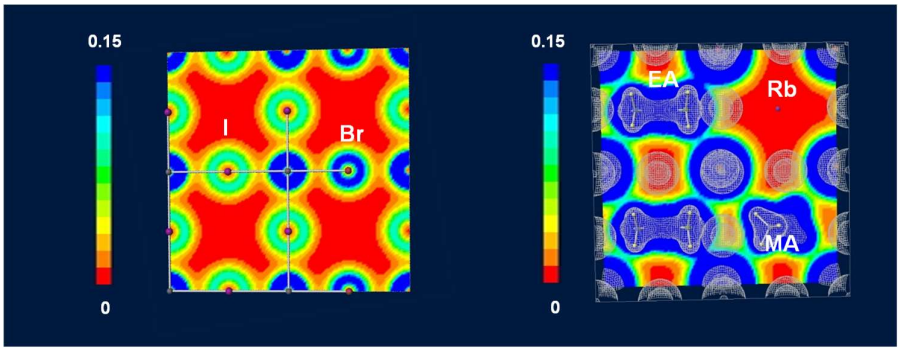

Figure 2. Electron density distribution of $MA_{0.625}EA_{0.25}Rb_{0.125}PbI_{2.25}Br_{0.75}$.

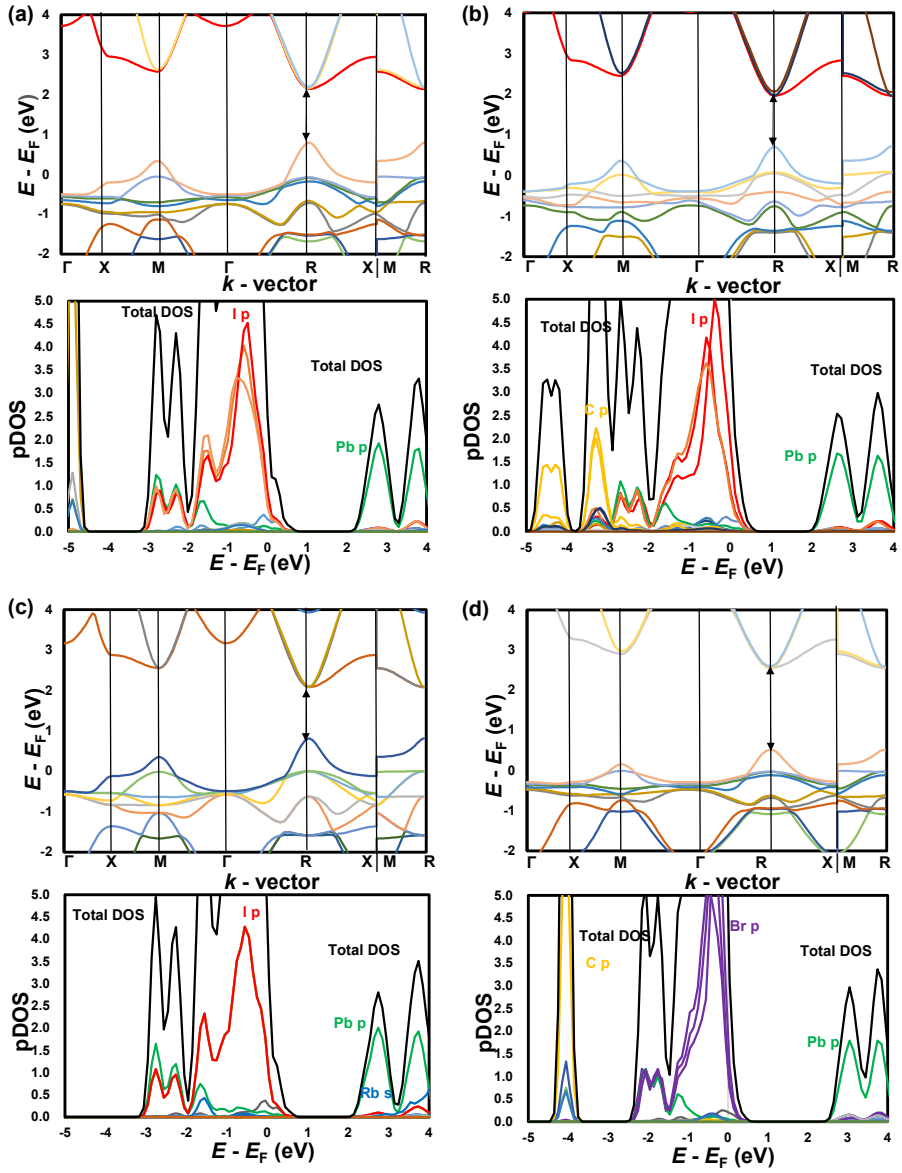

Figure 3. Band structures and DOS of (a) $MAPbI_3$ (b) $EAPbI_3$ (c) $RbPbI_3$ and (d) $MAPbBr_3$.

Figure 3 shows the results of band structure and DOS of four types of perovskites. Table 1 also summarizes the results of the effective masses and band gaps of electrons and holes calculated from the band calculations, and the total energies calculated from the first-principles calculations [43-46]. All crystals showed a direct transition type. I p orbitals dominate in the valence band and Pb p orbitals in the conduction band, while Rb s orbitals are found at higher energies than Pb b orbitals. The Rb s orbitals were localized at higher energies than the Pb b orbitals, which may contribute to the photovoltaic properties in the short wavelength regions due to optical absorption. The C p orbitals were found to be located far from the band edge. Compared to the $MAPbI_3$, the effective masses of electrons and holes in $EAPbI_3$, $RbPbI_3$, and $MAPbBr_3$ were smaller. The effective masses of electrons and holes became smaller in $EAPbI_3$, $RbPbI_3$ and $MAPbBr_3$ compared to the $MAPbI_3$. The effective masses of electrons and holes are smaller in $EAPbI_3$, $RbPbI_3$, and $MAPbBr_3$ than in $MAPbI_3$, suggesting an increase in carrier mobility. In addition, the band gap of $MAPbBr_3$ was greatly improved. This suggests an increase in the open-circuit voltage. The total energies were found to be stable with the substitution of EA and Br.

Table 1. Comparison of effective mass rations, energy gaps and total energies.

Device	Effective mass ratio		Energy gap E_g	Total energy
	m_e^*/m_0	m_h^*/m_0	(eV)	(eV cell^{-1})
$MAPbI_3$	0.055	0.031	1.391	-3483
$EAPbI_3$	0.049	0.024	1.241	-3682
$RbPbI_3$	0.050	0.028	1.268	-2999
$MAPbBr_3$	0.039	0.028	2.032	-3657

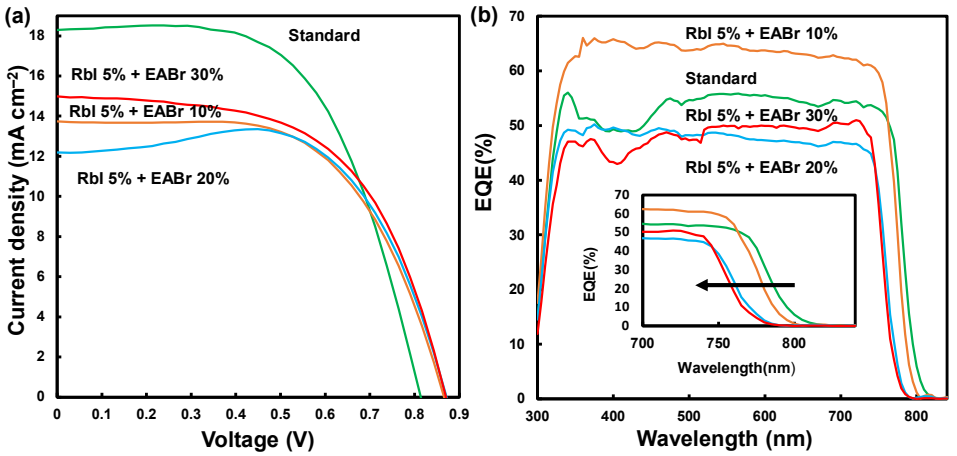

Figure 4. (a) *J-V* curves and (b) external quantum efficiencies of the devices.

Figure 4 and Table 2 shows the current density - voltage (*J-V*) curves and the external quantum efficiencies. The conversion efficiency was the highest for a standard device. The EQE is almost constant between 300 and 800 nm and shifts to shorter wavelengths with increasing EABr content around 800 nm. This is thought to have led to an increase in the open-circuit voltage by increasing the band gap.

Figure 5 shows the results of conversion efficiencies after 60 days. The conversion efficiencies of the standard device decreased from the initial value, probably due to the decomposition of perovskite by the desorption of MA, an organic substance, with time. However, in the doped systems, the conversion efficiencies were improved in all devices. Comparing each parameter, the improvement in J_{SC} and V_{OC} is remarkable. The reason for the improvement in conversion efficiency is thought to be the formation of crystals due to

ion diffusion inside the perovskite layer immediately after fabrication. The growth of these crystals by room temperature aging is thought to have improved the surface coverage and the interface between the TiO_2 layer and the perovskite layer, resulting in improved conversion efficiency.

Table 2. Measured photovoltaic parameters of solar cells.

Device	J_{SC} (mA cm^{-2})	V_{OC} (V)	FF	η (%)	η_{ave} (%)	R_s (Ω cm^2)	R_{sh} (Ω cm^2)	E_g (eV)
Standard	18.3	0.814	0.590	8.80	7.56	9.92	1427	1.55
RbI 5% + EABr 10%	13.7	0.866	0.602	7.16	5.92	13.1	1838	1.57
RbI 5% + EABr 20%	12.2	0.871	0.683	7.25	5.62	12.8	1698	1.60
RbI 5% + EABr 30%	15.0	0.869	0.576	7.51	6.44	10.8	1079	1.61
After 60 days	-	-	-	-	-	-	-	-
Standard	17.3	0.880	0.576	8.77	8.53	6.08	907	1.56
RbI 5% + EABr 10%	21.6	0.901	0.646	12.6	10.9	5.67	677	1.59
RbI 5% + EABr 20%	19.4	0.944	0.626	11.5	11.3	9.12	1030	1.61
RbI 5% + EABr 30%	17.7	0.933	0.622	10.3	9.89	7.99	1290	1.62

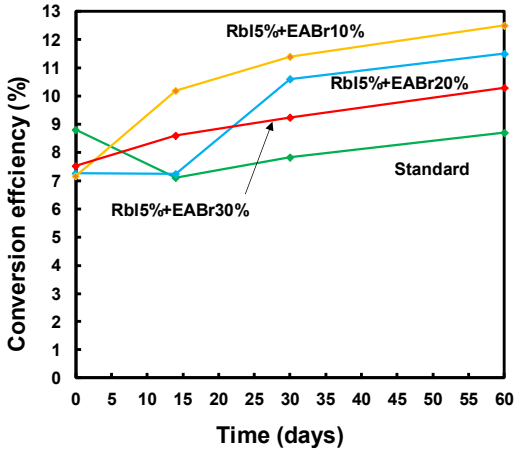

Figure 5. Changes in conversion efficiencies after 60 days in ambient air without encapsulation.

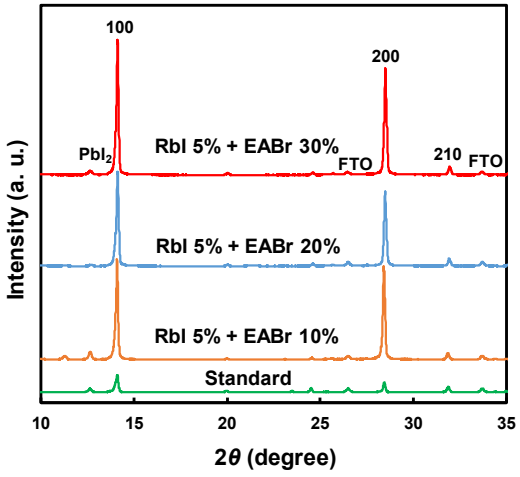

Figure 6. X-ray diffraction patterns of the devices.

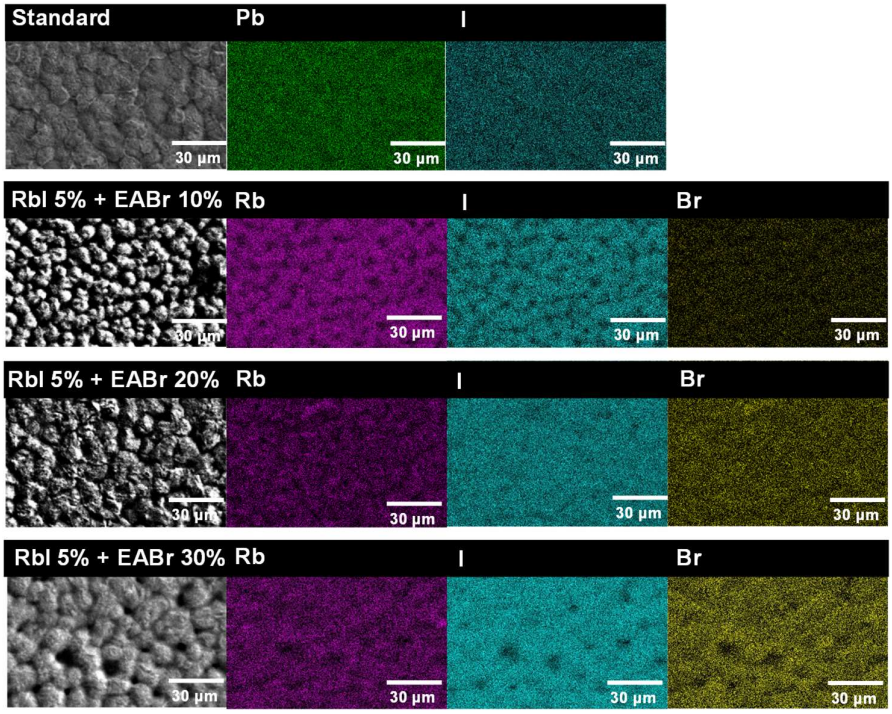

Figure 7. SEM images and elemental mapping images of the devices.

Figure 6 shows the results of the X-ray diffraction patterns, showing that the intensity of the perovskite peak is enhanced in the Rb and EA doped system. This suggests that the orientation of the perovskite crystals has been improved.

Figure 7 shows the results of SEM images and elemental mapping images of the perovskite layer; Surface of the standard device is smooth and. In the EA or Rb added system, the surface morphology is more dense, and the perovskite crystals are formed. The elemental mapping also shows that Rb, I and Br are distributed in the perovskite crystals.

4. Conclusions

The effects of EA and Rb addition on the photovoltaic properties were investigated using first-principles calculations and experimental devices. The first-principles calculations showed that the effective masses of electrons and holes are reduced by the addition of EA and Rb. It was also found that the band gap increases with the addition of bromine. When the amount of EABr was increased, the band gap was widened, which is consistent with the results of first-principles calculations. The open-circuit voltage was also improved accordingly. After two months, the conversion efficiency of the Rb and EA added devices was improved. The stability of the perovskite crystal was improved by the migration of Rb and EA to the position of the desorbed MA over time. The photovoltaic properties of the devices with simultaneous addition of EABr and RbI showed superior performance in terms of long-term stability compared to $MAPbI_3$ device.

Author Contributions: Conceptualization, K.T. and T.O.; Methodology, K.T., T.O., and A.S.; Formal Analysis, K.T., T.O., and A.S.; Investigation, K.T. and A.S.; Resources, M.O., S.F., T.T., and T.H.; Data Curation, K.T. and T.O.; Writing—Original Draft Preparation, K.T. and T.O.; Writing—Review & Editing, K.T., T.O., A.S., M.O., S.F., T.T., and T.H.; Project Administration, T.O.; Funding Acquisition, T.O.

Funding: This research was partly funded by a Grant-in-Aid for Scientific Research (C) 21K04809.

Conflicts of Interest: The authors declare no conflicts of interest.

References

1. Wang, Y.; Zhang, T.; Li, G.; Xu, F.; Li, Y.; Yang, Y.; Zhao, Y. A mixed-cation lead iodide $MA_{1-x}EA_xPbI_3$ absorber for perovskite solar cells. *J. Energy Chem.* **2018**, *27*, 215–218, doi:10.1016/j.jechem.2017.09.027.
2. Matsui, T.; Yokoyama, T.; Negami, T.; Sekiguchi, T.; Saliba, M.; Gratzel, M.; Sagawa, H. Effect of rubidium for thermal stability of triple-cation perovskite solar cells. *Chem. Lett.* **2018**, *12*, 814–816, doi.org/10.1246/cl.180211.
3. Zhang, M.; Yun, J.S.; Ma, Q.; Zheng, J.; Lau, C.F.J.; Deng, X.; Kim, J.; Kim, D.; Seidel, J.; Green, M.A.; Huang, S.; Ho-Bailie, A. High-efficiency rubidium-incorporated perovskite solar cells by gas quenching. *ACS Energy Lett.* **2017**, *2*, 438–444, doi:10.1021/acsenergylett.6b00697.
4. Fei, C.; Li, B.; Zhang, R.; Fu, H.; Tian, J.; Cao, G. Highly efficient and stable perovskite solar cells based on monolithically grained $CH_3NH_3PbI_3$ film. *Adv. Energy Mater*. **2017**, *7*, 1602017, doi:10.1002/aenm.201602017.
5. Tailor, N.; Abdi-Jalebi, M.; Gupta, V.; Hu, H.; Dar, M.; Satapathi, G.Li. Recent progress in morophology optimization in perovskite solar cell. *J. Mater. Chem. A*. **2020**, *8*, 21356–21386, doi:10.1039/d0ta00143k.
6. Alharbi, E.A.; Alyamani, A.Y.; Kubicki, D.J.; Uhl, A.R.; Walder, B.J.; Alanazi, A.Q.; Luo, J.; Burgos-Caminal, A.; Albadri, A.; Albrithen, H.; Hayal Alotaibi, M.; Moser, J.; Zakeeruddin, S, M.; Giordano, F.; Emsley, L.; Grätzel, M. Atomic-level passivation mechanism of ammonium salts enabling highly efficient perovskite solar cells. *Nat. Commun*. **2019**, *10*, 3008, doi.org/10.1038/s41467-019-10985-5, doi:10.1246/bcsj.20170208.
7. Yamada, Y.; Yamada, T.; Kanemitsu, Y. Free carrier radiative recombination and photon recycling in lead halide perovskite solar cell materials. *Bull. Chem. Soc. Jpn.* **2017**, *90*, 1129–1140, doi:10.1246/bcsj.20170208.
8. Liu, D.; Li, Q. Ethylammonium as an alternative cation for efficient perovskite solar cells from first-principles calculations. *RSC Adv.* **2019**, *9*, 7356–7361, doi:10.1039/c9ra00853e.
9. Solanki, A.; Yadav, P.; Turren-Cruz, S, H.; Lim, S, S.; Salibac, M.; Sum, T, C. Cation influence on carrier dynamics in perovskite solar cells. *Nano Energy*. **2019**, *58*, 604–611, doi:10.1016/j.nanoen.2019.01.060.
10. Tu, Y.; Wu, J.; Lan, Z.; He, X.; Dong, J.; Jia, J.; Guo, P.; Lin, J.; Huang, M.; Huang, Y. Modulated $CH_3NH_3PbI_{3-x}Br_x$ film for efficient perovskite solar cells exceeding 18%. *Sci. Rep*. **2017**, *7*, 444603, doi:10.1038/srep44603.
11. Huang, S.H.; Guan, C.K.; Lee, P.H.; Huang, H.C.; Li, C.F.; Huang, Y.C.; Su, W. Toward All Slot-Die Fabricated high efficiency large area perovskite solar cell using rapid near infrared heating in ambient air. *Adv. Energy Mater*. **2020**, 2001567, doi:10.1002/aenm.202001567.
12. Lee, H.; Kumar, N.; Tyagi, B.; He, S.; Sahani, R.; Kang, J, W. Bulky organic cations engineered lead-halide perovskites: a review on dimensionality and optoelectronic applications. *Mater. Today Energy* **2021**, *21*, 100759, doi:10.1016/j.mtener.2021.100759.
13. Wu, T.; Qin, Z.; Wang, Y.; Wu, Y.; Chen, W.; Zhang, S.; Cai, M.; Dai, S.; Zhang, J.; Liu, J.; Zhou, Z.; Liu, X.; Segawa, H.; Tan, T.; Tang, Q.; Fang, J.; Li, Y.; Ding, L.; Ning, Z.; Qi, Y.; Zhang, Y.; Han, L. The main progress of perovskite solar cells in 2020–2021. *Nano-Micro Lett*. **2021**, *13*, 152. doi:10.1007/s40820-021-00672-w.
14. Pitriana, P.; Wungu, T.; Hidayat, R.; Herman, H. Ab-initio calculation of $APbI_3$ (A=Li, Na, K, Rb and Cs) perovskite crystal and their lattice constants optimization using density functional theory. J. Phys. Conf. Series **2019**, *1170*, 012023, doi:10.1088/1742-6596/1170/1/012023.
15. Ueoka, N.; Oku, T.; Suzuki, A. Effects of doping with Na, K, Rb, and formamidinium cations on $(CH_3NH_3)_{0.99}Rb_{0.01}Pb_{0.99}Cu_{0.01}I_{3-x}(Cl, Br)_x$ perovskite photovoltaic cells. *AIP Adv.* **2020**, *10*, 125023, doi:10.1063/5.0029162.
16. Ke, W.; Kanatzidis, M.G. Prospects for low-toxicity lead-free perovskite solar cells. *Nat. Commun.* **2019**, 10, 965–969, doi:10.1038/s41467-019-08918-3.
17. Oku, T. Crystal structures of perovskite halide compounds used for solar cells. *Rev. Adv. Mater. Sci.* **2020**, *59*, 264–305, doi:10.1515/rams-2020-0015.
18. Ueoka, N.; Oku, T.; Suzuki, A. Additive effects of alkali metals on Cu-modified $CH_3NH_3PbI_{3-\delta}Cl_\delta$ photovoltaic devices. *RSC Adv.* **2019**, *9*, 24231–24240, doi:10.1039/c9ra03068a.
19. Suzuki A.; Oe M.; Oku T., Fabrication and characterization of Ni-, Co-, and Rb-incorporated $CH_3NH_3PbI_3$ perovskite solar cells, *J. Electronic Mater.* **2021**, *50*, 1980–1995. https://doi.org/10.1007/s11664-021-08759-1.
20. Machiba, H.; Oku, T.; Kishimoto, T.; Ueoka, N.; Suzuki, A. Fabrication and evaluation of K-doped $MA_{0.8}FA_{0.1}K_{0.1}PbI_3(Cl)$ perovskite solar cells. *Chem. Phys. Lett.* **2019**, *730*, 117–123, doi:10.1016/j.cplett.2019.05.050.
21. Kandori, S.; Oku, T.; Nishi, K.; Kishimoto, T.; Ueoka, N.; Suzuki, A. Fabrication and characterization of potassium- and formamidinium-added perovskite solar cells. *J. Ceram. Soc. Jpn.* **2020**, *128*, 805, doi:10.2109/jcersj2.20090.
22. Ueoka, N.; Oku, T. Effects of co-addition of sodium chloride and copper (II) bromide to mixed-cation mixed-halide perovskite photovoltaic devices. *ACS Appl. Energy Mater.* **2020**, *3*, 7272–7283, doi:10.1021/acsaem.0c00182.
23. Suzuki, A.; Kato, M.; Ueoka, N.; Oku, T. Additive effect of formamidinium chloride in methylammonium lead halide compound-based perovskite solar cells. *J. Electron. Mater.* **2019**, *48*, 3900–3907, doi:10.1007/s11664-019-07153-2.
24. Nishi, K.; Oku, T.; Kishimoto, T.; Ueoka, N.; Suzuki, A. Photovoltaic characteristics of $CH_3NH_3PbI_3$ perovskite solar cells added with ethylammonium bromide and formamidinium iodide. *Coatings* **2020**, *10*, 410, doi:10.3390/coatings10040410.
25. Chu, Z.; Zhao, Y.; Ma, F.; Zhang, C.X.; Deng, H.; Gao, F.; Ye, Q.; Meng, J.; Yin, Z.; Zhang, X.; You, J. Large cation ethylammonium incorporated perovskite for efficient and spectra stable blue light-emitting diodes. *Nat. Commun.* **2020**, *11*, 4146, doi:10.1038/s41467-020-17943-6.

26. Mateen, M.; Arain, Z.; Liu, X.; Iqbal, A.; Ren, Y.; Zhang, X.; Liu, C.; Chen, Q.; Ma, S.; Ding, Y.; Cai, M.; Dai, S. Boosting optoelectronic performance of $MAPbI_3$ perovskite solar cells via ethylammonium chloride additive engineering. *Sci. China Mater.* 2020, *63*, 2477–2486, doi:10.1007/s40843-020-1383-3.
27. Kishimoto, T.; Suzuki, A.; Ueoka, N.; Oku, T. Effects of guanidinium addition to $CH_3NH_3PbI_{3-x}Cl_x$ perovskite photovoltaic devices. *J. Ceram. Soc. Jpn.* **2019**, *127*, 491−497, doi:10.2109/jcersj2.18214.
28. Kishimoto, T.; Oku, T.; Suzuki, A.; Ueoka, N. Additive effects of guanidinium iodide on $CH_3NH_3PbI_3$ perovskite solar cells. *Phys. Status Solidi A* **2021**, *218*, 2100396. doi:10.1002/pssa.202100396.
29. Ono, I.; Oku, T.; Suzuki, A.; Asakawa, Y.; Terada, S.; Okita, M.; Fukunishi, S.; Tachikawa, T. Fabrication and characterization of $CH_3NH_3PbI_3$ solar cells with added guanidinium and inserted with decaphenylpentasilane, *Jpn. J. Appl. Phys.* **2021,** doi: 10.35848/1347-4065/ac2661.
30. Oku, T.; Ohishi, Y. Effects of annealing on $CH_3NH_3PbI_3$(Cl) perovskite photovoltaic devices. *J. Ceram. Soc. Jpn.* **2018**, *126*, 56−60, doi:10.2109/jcersj2.17162.
31. Liao, K.; Li, C.; Xie, L.; Yuan, Y.; Wang, S.; Cao, Z.; Ding, L.; Hao, F. Hot-casting large-grain perovskite film for efficient solar cells: film formation and device performance. *Nano-Micro Lett*. **2021**, *12*, 156, doi:10.1007/s40820-020-00494-2.
32. Wang, M.; Wang, W.; Ma, B.; Shen, W.; Liu, L.; Cao, K.; Chen, S.; Huang, W. Lead-free perovskite materials for solar cells. *Nano-Micro Lett*. **2021**, *13*, 62, doi:10.1007/s40820-020-00578-z.
33. Shao, S.; Dong, J.; Duim, H.; Brink, G.H.; Blake, G.R.; Portale, G.; Loi, M.A. Enhancing the crystallinity and perfecting the orientation of formamidinium tin iodide for highly efficient Sn-based perovskite solar cells. *Nano Energy* **2019**, *60*, 810–816, doi.org/10.1016/j.nanoen.2019.04.040.
34. Zhang, Y.; Kim, S.G.; Lee, D.; Shin, H.; Park, N.G. Bifacial stamping for high efficiency perovskite solar cells. *Energy Environ. Sci.* **2018**, doi:10.1039/c8ee02730g.
35. Lee, J.W.; Kim, S.G.; Yang, J.M. Verification and mitigation of ion migration in perovskite solar cells. *APL Mater*. **2019**, *7*, 041111, doi:10.1063/1.5085643.
36. Oku, T.; Zushi, M.; Imanishi, Y.; Suzuki, A.; Suzuki, K. Microstructures and photovoltaic properties of perovskite-type $CH_3NH_3PbI_3$ compounds. *Appl. Phys. Express* **2014**, *7*, 121601, doi:10.7567/APEX.7.121601.
37. Oku, T.; Ohishi, Y.; Ueoka, N. Highly (100)-oriented $CH_3NH_3PbI_3$(Cl) perovskite solar cells prepared with NH_4Cl using an air blow method. *RSC Adv*. **2018**, *8*, 10389–10395, doi:10.1039/c7ra13582c.
38. Taguchi, M.; Suzuki, A.; Oku, T.; Ueoka, N.; Minami, S.; Okita, M. Effects of annealing temperature on decaphenylcyclopentasilane-inserted $CH_3NH_3PbI_3$ perovskite solar cells. *Chem. Phys. Lett.* **2019**, *737*, 136822, doi:10.1016/j.cplett.2019.136822.
39. Oku, T.; Kandori, S.; Taguchi, M.; Suzuki, A.; Okita, M.; Minami, S.; Fukunishi, S.; Tachikawa, T. Polysilane-inserted methylammonium lead iodide perovskite solar cells doped with formamidinium and potassium. *Energies* **2020**, *13*, 4776, doi:10.3390/en13184776.
40. Suzuki A.; Taguchi M.; Oku T.; Okita M.; Minami S.; Fukunishi S.; Tachikawa T., Additive effects of methyl ammonium bromide or formamidinium bromide in methylammonium lead iodide perovskite solar cells using decaphenylcyclopentasilane, *J. Mater. Sci.: Mater. Electron.* **2021**, *32*, 26449–26464, doi:10.1007/s10854-021-07023-w.
41. Oku, T.; Taguchi, M.; Suzuki, A.; Kitagawa, K.; Asakawa, Y.; Yoshida, S.; Okita, M.; Minami, S.; Fukunishi, S.; and Tachikawa, T.; Effects of polysilane addition to chlorobenzene and high temperature annealing on $CH_3NH_3PbI_3$ perovskite photovoltaic devices. *Coatings* **2021**, *11*, 665, doi:10.3390/coatings11060665.
42. Han, T.H.; Lee, J.W.; Choi, C.; Tan, S.; Lee, C.; Zhao, Y.; Dai, Z.; Marco, N.D.; Lee, S.J.; Bae, S.H.; Yuan, Y.; Mo Lee, H.; Yu Huang and Yang, Y.; Perovskite-polymer composite cross-linker approach for highly-stable and efficient perovskite solar cells. *Nat. Commun*. **2019**, *10*, 520, doi:10.1038/s41467-019-08455-z.
43. Suzuki A.; Oku T., First-principles calculation study of electronic structures of alkali metals (Li, K, Na and Rb)-incorporated formamidinium lead halide perovskite compounds, *Appl. Surf. Sci.* **2019**, *483*, 912-921. doi:10.1016/j.apsusc.2019.04.049.
44. Suzuki A.; Miyamoto Y.; Oku T., Electronic structures, spectroscopic properties, and thermodynamic characterization of sodium- or potassium-incorporated $CH_3NH_3PbI_3$ by first-principles calculation *J. Mater. Sci.* **2020**, *55*, 9728–9738. doi:10.1007/s10853-020-04511-y.
45. Suzuki A.; Oku T., Effects of mixed-valence states of Eu-doped $FAPbI_3$ perovskite crystals studied by first-principles calculation, *Mater. Adv.*, **2021**, 2, 2609–2616. doi:10.1039/D0MA00994F.
46. Suzuki A.; Kitagawa K.; Oku T.; Okita M.; Fukunishi S.; Tachikawa T., Additive effects of copper and alkali metal halides into methylammonium lead iodide perovskite solar cells, *Electron. Mater. Lett.* **2021**, doi:10.1007/s13391-021-00325-5.